Journal of Materials Chemistry A

Accepted Manuscript

ROYAL SOCIETY OF CHEMISTRY

www.rsc.org/materialsA

Journal Name

ARTICLE

Enhancement of Anisotropic Thermoelectric Performance of Tungsten Disulfide by Titanium Doping

Received 00th January 20xx,
Accepted 00th January 20xx

DOI: 10.1039/x0xx00000x

www.rsc.org/

Zhiwei Huang,[a, d, §] Tianmin Wu,[c, §] Shuang Kong,[a,d] Qing-Long Meng,[a] Wei Zhuang,[*, b, e] Peng Jiang,[*, a] Xinhe Bao[*,a]

Thermoelectric power generator, as one promising renewable energy resource, has attracted intense attention over past few decades. However, the large-scale employment of thermoelectric convertors relies on the cost-effective and eco-friendly thermoelectric materials with decent efficiency. For transition metal dichalcogenide semiconductors (TMDCs), a potential thermoelectric material, the thermoelectric efficiency is hampered by their poor intrinsic electrical conductivities. Herein, we demonstrate that the thermoelectric performance of WS_2, a typical TMDC material, can be dramatically enhanced up to 70 times by doping titanium. The anisotropic thermoelectric properties of these layered WS_2 structures were also revealed systematically. The realization of decent thermoelectric efficiency on WS_2 by facile doping strategy will stimulate future explorations of thermoelectric applications for other TMDCs and layered materials.

1 Introduction

Two-dimensional transition metal dichalcogenide semiconductors (TMDCs) have recently attracted intense attention due to their unique electronic and optical properties.[1] A rarely explored property of TMDCs, however, is their plausible potential as the nontoxic and earth-abundant thermoelectric materials.[2] The thermoelectric efficiency is characterized by the figure of merit $ZT=(S^2\sigma/\kappa)T$, where S, σ, κ and T are the Seebeck coefficient, electrical conductivity, thermal conductivity and absolute temperature of materials, respectively.[3] Unlike the gapless graphene, which has the insignificant ZT value due to its miserable Seebeck coefficient and the extremely large thermal conductivity,[4] TMDCs hold great promise for thermoelectric applications given the tunable bandgap, decent Seebeck coefficient and small cross-plane thermal conductivity.[2a,2b,5] Recent theoretical calculation predicted that for p-type WS_2, a typical TMDC material, it is possible to reach the maximum cross-plane ZT value of 0.77 at 1500 K with optimized carrier concentrations about 10^{19} cm^{-3}.[5] Gandi and Schwingenschlogl further revealed that the layered structure of WS_2 shows the evident anisotropic thermoelectric performance because of its strong interlayer bonding and weak van der Vaals cross-layer interaction. They predicted that the maximum in-plane ZT is only 0.4 at 1000 K for p-type WS_2, and the inferior in-plane ZT is due to the high in-plane thermal conductivity.

The experimental realization of high ZT values in TMDCs is, however, hampered by the intrinsically low electrical conductivity, which is usually at the level of 1 S m^{-1}, much lower than what is required for a good thermoelectric material. [6] We herein demonstrate that, by doping WS_2 with titanium, its electrical conductivity can be dramatically enhanced, which leads to a significant improvement of the power factor $S^2\sigma$. At the same time, the thermal conductivity along the cross-plane direction of the titanium doped WS_2 is reduced. As a result, the maximum ZT can be enhanced for up to 70 times. Further study reveals that, due to the smaller thermal conductivity, the cross-plane thermoelectric performance is much superior than the in-plane one. The facile and effective doping scheme therefore provides a general guidance to explore novel thermoelectric materials based on TMDCs as well as other layered materials.

2 Experimental section

2.1 Synthesis

Ti_xWS_2 (x=0, 0.02, 0.05, 0.1, 0.15 and 0.20) composites were prepared by spark plasma sintering (SPS) method. Ti powder (99.99%, 325 mesh, Alfa Aesar) and WS_2 powder (99.8%, Alfa Aesar) were weighed in specific mole ratio (0, 0.02, 0.05, 0.1, 0.15 and 0.20) and ground for 90 min using a mortar. Then the mixtures of Ti and WS_2 were put into a graphite die and sintered using a SPS system (Labox-650F) at 1500℃ for 10 min under a mechanical pressure of 50 MPa. Then the samples were cooled to room

[a] State Key Laboratory of Catalysis, CAS Center for Excellence in Nanoscience, Dalian Institute of Chemical Physics, Chinese Academy of Sciences, Dalian, Liaoning 116023, China. E-mail: pengjiang@dicp.ac.cn, xhbao@dicp.ac.cn
[b] State Key Laboratory of Structural Chemistry, Fujian Institute of Research on the Structure of Matter, Chinese Academy of Sciences, Fuzhou, Fujian 350002, China. E-mail: wzhuang@fjirsm.ac.cn
[c] Department of Chemical Physics, University of Science and Technology of China, Hefei, Anhui 230026, China
[d] University of Chinese Academy of Sciences, Beijing, 100049, China
[e] State Key Laboratory of Molecular Reaction Dynamics, Dalian Institute of Chemical Physics, Chinese Academy of Sciences, Dalian, Liaoning 116023, China
Electronic Supplementary Information (ESI) available: [details of any supplementary information available should be included here]. See DOI: 10.1039/x0xx00000x

temperature naturally. The ingots obtained from sintering were 12.7 mm in diameter and 10 mm in thickness. The obtained pellets were polished and cut into bars with specific shape and size for thermoelectric properties measurements.

2.2 Thermoelectric properties measurements

To check the anisotropy, thermoelectric properties were measured along two directions: perpendicular and parallel to the pressing directions. The pellets were cut into rectangular bars in dimension of 8×2×2 mm^3 for measurements of electrical properties. The electrical conductivity and Seebeck coefficient were measured by a thermoelectric measurement system (ZEM-3 ULVAC, Japan) from 323 K to 1000 K in helium atmosphere. Electrical properties were measured using four probes method. The uncertainty of electrical properties measurements is 5%.

Thermal conductivity (κ_{tot}) was calculated using $\kappa_{tot}=D*Cp*\rho$, where D is the thermal diffusivity coefficient, C_p is the heat capacity, ρ is the density. Thermal diffusivity coefficient was measured by a laser flash analysis system (LFA 457, Netzsch) from 323 K to 1000 K under continuous helium flow. The samples used for parallel direction were coins with 12.7 mm diameter and 2 mm thickness. The bars used for perpendicular direction were square in dimension of 6×6×2 mm^3. All samples were coated with a thin graphite layer before thermal diffusivity coefficient measurements. Heat capacity (C_p) was measured using a differential scanning calorimeter (STA 449 F3, Netzsch) from 323 K to 1073 K at a heating rate of 10 K/min in N_2 atmosphere. Sapphire was used as reference. Density was calculated using $\rho=m/V$, where m is the mass of sample, V is the volume of sample. The lattice thermal conductivity κ_{lat} was calculated from $\kappa_{lat}=\kappa_{tot}-\kappa_{ele}$. The electrical thermal conductivity was calculated using $\kappa_{ele}=L\sigma T$, where L is the Lorenz number, σ is the electrical conductivity, T is the temperature. The Lorenz number L was calculated from the following equation: [7]

$$L = 1.5 + exp[-\frac{|S|}{116}] \quad (1)$$

where S is the Seebeck coefficient.

2.3 Characterization

The microstructure and elemental mapping was characterized by a scanning electron microscope (QUANTA 200 FEG). The phase structure was investigated by a X-ray diffraction instrument (Empyrean) using Cu Kα radiation at room temperature. Carrier concentration and carrier mobility were measured using a Hall system (HL5500PC) at 323 K.Transmission electron microscope images were obtained by a JEM-2100 system.

2.4 Theoretical calculations.

First-principles calculations of the pristine WS_2 have been conducted using density functional theory (DFT) method implemented in the Vienna ab initio simulation package (VASP).[8] The projector-augmented-wave (PAW) pseudopotentials and generalized gradient approximation of Perdew-Burke-Ernzerhof (PBE) for exchange and correlation were adopted in our simulations.[9] Furthermore, the van der Waals interactions were taken into account by the semi-empirical correction of Grimme.[10] The plane-wave cutoff was chosen as 500 eV, all atomic coordinates were relaxed until the forces on the atoms have declined to 0.01 eV $Å^{-1}$, enforcing a total energy convergence criterion of 1×10^{-5} eV. In order to describe the band gap of system correctly, the computationally expensive hybrid functional approach of Heyd, Scuseria, and Ernzerhof (HSE06) was used with 25% Hartree-Fock exchange and μ=0.4 $Å^{-1}$.[11] Semi-classical Boltzmann transport theory[12] was used to calculate the temperature- and doping-dependent thermoelectric properties with the constant scattering time approximation (CSTA), and the rigid band approach as implemented in the BoltzTraP code.[13] As mentioned, the calculations of thermoelectric properties can be very sensitive to the Brillouin zone sampling especially for low doping levels and low temperature, we calculated the electronic structures required for the transport calculations with very dense 43 × 43 × 11 k-point meshes in Brillouin zone (BZ). A super cell with 2 × 2 × 1 with 24 atoms was built for the purpose of randomly replacing one W atom with Ti atom (TiW_7S_{16}) to simulate the experimental operation. A Monkhorst–Pack k-mesh scheme with 9 × 9 × 5 and 15 × 15 × 7 was used to calculate the total energy and DOS, respectively.

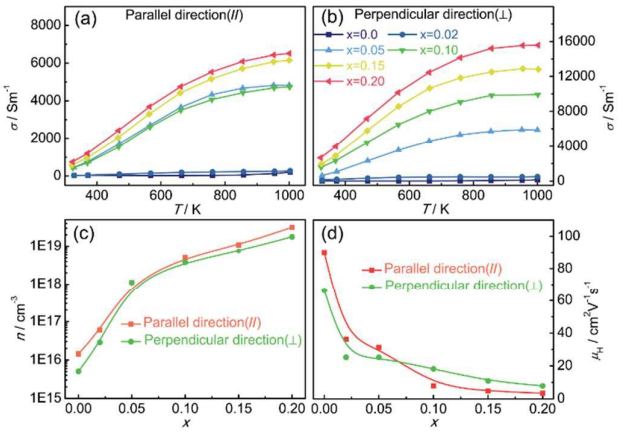

Fig. 1 Temperature dependent electrical conductivity (a,b) for Ti_xWS_2 (x=0, 0.02, 0.05, 0.1, 0.15, 0.2) along both directions parallel and perpendicular to the pressing direction. c) Carrier concentration versus titanium mole ratio (x). d) Carrier mobility versus titanium mole ratio.

3 Results and discussion

3.1 Electrical transport properties of Ti_xWS_2

Fig. 1(a and b) show the temperature dependent electrical conductivities of Ti_xWS_2 parallel and perpendicular to the pressing directions. The room temperature $\sigma_{//}$ (parallel to the pressing direction) and $\sigma_{\perp}$ (perpendicular to the pressing direction) of pristine WS_2 is 25 S m^{-1} and 9 S m^{-1}, respectively, which is consistent with the literature values but too low for thermoelectric applications.[6] With Ti doping, the electrical conductivity increases continuously with doping amount. At the room temperature, $\sigma_{//}$ and $\sigma_{\perp}$ can reach 746 S m^{-1} and 2667 S m^{-1} with 20% Ti doping, respectively. The increment of the electrical conductivity observed

is attributed to the pronounced increase of the carrier concentration by Ti doping. As shown in Fig. 1c, the carrier concentration increases from 10^{15} cm^{-3} for pristine WS_2 to 10^{19} cm^{-3} for $Ti_{0.2}WS_2$ along both directions. With the increase of the carrier concentration, the impurity scattering probability is also increased, leading to the reduction of the mobility from 90 and 66 cm^2 V^{-1} S^{-1} (pristine WS_2) to 3.4 and 7.9 cm^2 V^{-1} S^{-1} ($Ti_{0.2}WS_2$) along two directions at 300 K (Fig. 1(d)). It is apparent that the gain on carrier concentration overcomes the decrease of mobility, leading to an overall increase of electrical conductivity by doping.

Based on the theoretical calculation, as demonstrated in Fig. S3, compared with pristine WS_2 (Fig. S3(a)), heavy Ti doping (Fig. S3(b)) apparently shifts the position of Fermi level into the valance band and flattens the valance band. The shift of Fermi level into the valance band indicates that Ti doping is p-type doping, which is consistent with experimental result, while the flattened valance band give arise to increasing the effective mass of holes.[14] Furthermore, Ti doping also modifies the profile of DOS, especially the local DOS near the Fermi level, which can greatly increase the carrier concentration and the electronic conductivity, since the carrier concentration $n(E) = f(E)g(E)$, $f(E)$ is the Fermi distribution function and $g(E)$ is the density of state, which depends on the energy derivative of the energy-dependent DOS.

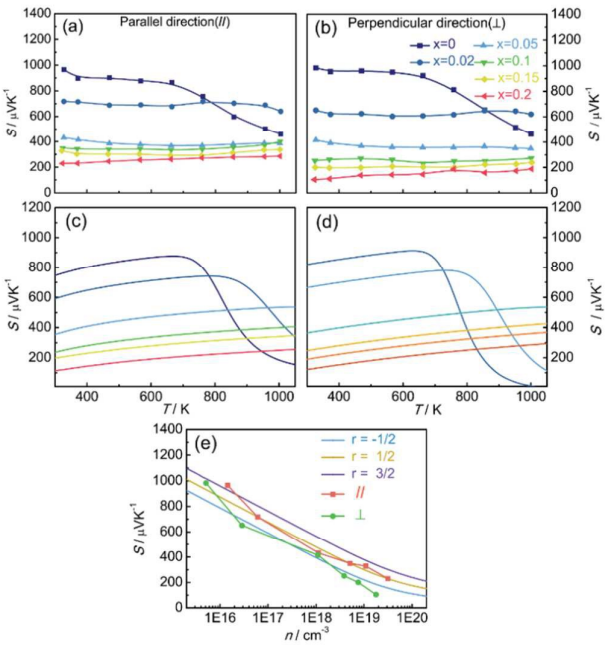

Fig. 2 Temperature-dependent Seebeck coefficients (a) and (b) for Ti_xWS_2 (x=0, 0.02, 0.05, 0.1, 0.15, 0.2) and the corresponding theoretical results (c) and (d) along both directions. (e) Carrier concentration dependence of Seebeck coefficient. The solid curves are the calculated Seebeck coefficients at 327 K versus carrier concentration when *r* equals to -1/2, 1/2 and 3/2 respectively. The red square and green circle points are the experimental data parallel and perpendicular to the pressing directions, respectively.

Due to the anisotropy of band structure induced by the anisotropic two-dimensional nature of layered structures, the electrical conductivities of WS_2 are theoretically predicted to exhibit evident anisotropic behavior.[5] However, we observed that the pristine WS_2 and Ti-doped WS_2 samples exhibit more complex anisotropic behaviors than expected. For the pristine WS_2, $\sigma_{//}$ is larger than $\sigma_{\perp}$, while for highly doped WS_2, $\sigma_{\perp}$ is larger than $\sigma_{//}$. In the case of pristine samples, $\sigma_{\perp}$ at 1000 K is about 138 S m^{-1}, while $\sigma_{//}$ is about 199 S m^{-1}, resulting in an anisotropy factor ($\sigma_{\perp}/\sigma_{//}$) about 0.69. Interestingly, with the increase of Ti doping amount, the anisotropic trend is reversed at certain doping level. For example, in the case of $Ti_{0.2}WS_2$, $\sigma_{\perp}$ at 1000 K is about 15571 S m^{-1}, while $\sigma_{//}$ is only about 6514 S m^{-1}, resulting in an anisotropy factor ($\sigma_{\perp}/\sigma_{//}$) about 2.39. The change of anisotropy in electrical conductivities can be explained by the structure changes with doping, which will be discussed later in this paper.

The electrical conductivity increases with temperature for all samples, suggesting a semiconducting transport behavior. However, the pristine and doped samples exhibit some distinct differences. For the pristine WS_2, the conductivities do not depend strongly on the temperature below 750 K, but when the temperature is above 750 K, the conductivities increase exponentially with temperature. This phenomenon could be explained by the thermal excitation of charge carriers, for which the temperature needs to be higher than certain threshold. For doped WS_2, the electrical conductivity significantly increases with temperature in all temperature range. At the same temperature, the electrical conductivity increases with further doping due to the higher carrier concentration. Furthermore, the increasing rate of electrical conductivity is reduced in the high temperature regime, which is probably due to the intensified phonon and impurity scattering.

3.2 Seebeck coefficient.

Fig. 2(a and b) show the experimental Seebeck coefficients parallel and perpendicular to the pressing directions as the function of temperature. The positive Seebeck coefficients indicate the p-type conduction. With increasing Ti concentration, the Seebeck coefficient decreases continuously. As mentioned above, doping Ti will increase the carrier concentration (Fig. 1(c)). Fig. 2(e) represents the dependence of Seebeck coefficient on carrier concentration for Ti_xWS_2. In the electron relaxation time model, the Seebeck coefficient in the degenerate doping limit is given by:[15]

$$S = \frac{k_B}{e}\frac{\pi^2}{3}\frac{k_B T}{\varepsilon_F}\left(\frac{3}{2} + r\right) \qquad (2)$$

Where ε_F is the Fermi level, k_B is the Boltzmann constant, and *r* is the index of the electron relaxation time related to kinetic energy. As shown in Fig. 2(e), the Seebeck coefficient along the direction parallel to the pressing direction decreases along the *r*=1/2 curve as the titanium doping concentration increases, which indicates that the Ti atoms might be embedded into the system of WS_2 but have weak interaction with both atom of W and S. Therefore, the electron transport along this direction is dominated by the neutral impurity scattering mechanism. While for the perpendicular direction, due to the weak interaction induced by the doped atom

of Ti, the Seebeck coefficient decreases along the r=-1/2 curve as the carrier concentration increases, suggesting that the electron transport mechanism along this direction is phonon-scattering-controlled. It needs to be emphasized that, compared with evident anisotropic behavior of electrical conductivities, the Seebeck coefficients only show minor anisotropy. This unobvious anisotropic behavior of Seebeck coefficient is consistent with the observation on other textured thermoelectric materials, like Bi_2Te_3 and BiCuSeO.[16]

The trends of experimental Seebeck coefficients with temperature for each doping concentration are consistent with theoretical results, as presented in Fig. 2(c and d). For pristine WS_2, the Seebeck coefficients along both directions remain almost constant in the 300-700 K temperature range but sharply drop above 750 K. In correspondence with trends of electrical conductivity with temperature as discussed above (Fig. 1(a and b)), the low thermal excited carrier concentration have little effect on the Seebeck coefficient below 750 K. However, a large number of thermal excited carriers are generated above 750 K, leading to the increase of electrical conductivities and the decrease of Seebeck coefficients.

In contrast to the pristine WS_2, both experimental data and theoretical simulation show the Seebeck coefficients of Ti doping WS_2 along each direction remain almost stable as temperature increases. The effect of thermally excited carriers on Seebeck coefficient is not pronounced at high doping concentration because of the limited amount of thermally excited carriers in comparison with the dominant charge carriers from doping.

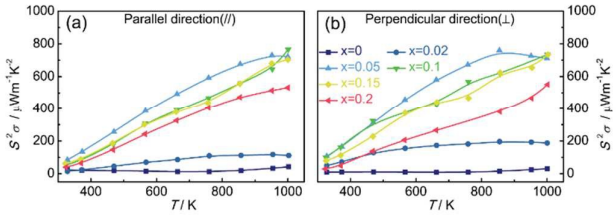

Fig. 3 Temperature-dependent power factors for Ti_xWS_2 (x=0, 0.02, 0.05, 0.1, 0.15, 0.2) along both parallel and perpendicular to the pressing directions.

The combination of the enhanced electrical conductivity and decent Seebeck coefficient by Ti doping results in a dramatic enhancement of the power factor (PF=$S^2\sigma$), which is shown in Fig. 3(a and b). For the pristine WS_2 sample, the PF value at 1000 K is around 40 μW m^{-1} K^{-2}, while after doping with 10% Ti, the PF is greatly improved up to 750 μW m^{-1} K^{-2} at 1000 K. Due to the nearly isotropic Seebeck coefficient, there is no clear anisotropy for power factors, even the electrical conductivity exhibiting distinct anisotropic behavior.

3.3 Thermal transport properties of Ti_xWS_2

The temperature-dependent thermal conductivities of Ti_xWS_2 along both directions are presented in Fig. 4. The thermal conductivities of all samples decrease with the increase of temperature, suggesting that the Umklapp scattering mechanism dominates the phonon scattering.[17] By subtracting the electronic thermal conductivity (κ_{ele}) using Wiedemann-Franz relation $\kappa_{ele}=L\sigma T$,[3a] where L is the Lorenz number, it is evident that the phonon thermal conductivity dominates the overall thermal conductivity for both directions, as show in Fig. 4(c and d).

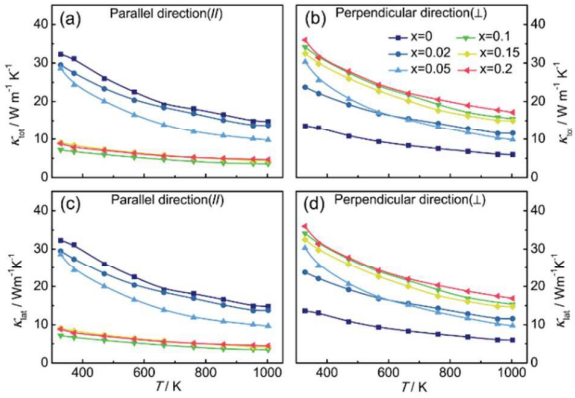

Fig. 4 Temperature-dependent (a,b) total thermal conductivity, (c,d) lattice thermal conductivity for Ti_xWS_2(x=0, 0.02, 0.05, 0.1, 0.15, 0.20) along both directions.

It is worth noting that, for the pristine WS_2 sample, the thermal conductivity in the direction perpendicular to the pressing direction ($\kappa_\perp$) is smaller than the thermal conductivity in the direction parallel to the pressing direction ($\kappa_{//}$), which is in contrast with the other TMDCs. Furthermore, with increasing Ti fraction, the thermal conductivities along two directions exhibit an opposite trend. $\kappa_\perp$ increases with doping, while $\kappa_{//}$ decreases with doping. When the concentration of Ti is above 10%, there is a crossover, where $\kappa_{//}$ becomes smaller than $\kappa_\perp$. The abnormal behavior of the thermal conductivity of pristine WS_2 and the evolution of thermal conductivity with Ti doping are consistent with the electrical transport properties (Figure 1(a and b)) and can be explained based on the structure information from XRD and SEM results.

Fig. 5 Temperature dependent thermoelectric figure of merit (ZT)

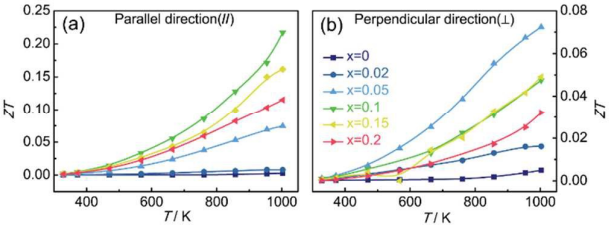

for Ti_xWS_2(x=0, 0.02, 0.05, 0.1, 0.15, 0.20) along both directions.

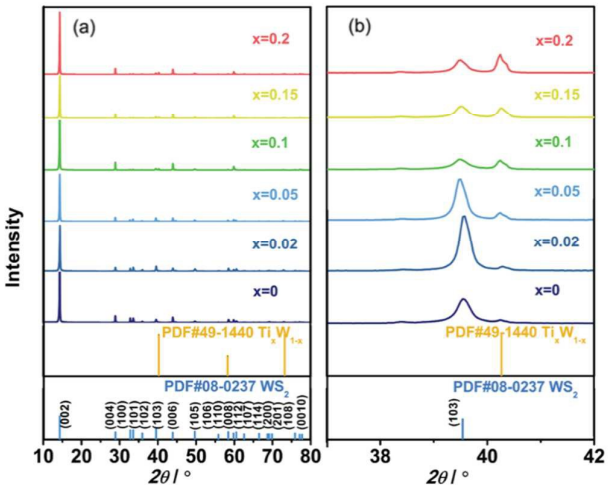

Fig. 6 (a) XRD patterns for Ti_xWS_2(x=0, 0.02, 0.05, 0.1, 0.15, 0.20) along the direction parallel to the pressing direction ,(b) an enlarged view of XRD patterns around TiW alloy peak.

3.4 Improved thermoelectric figure of merit *ZT* by doping Ti

Fig. 5 shows the temperature-dependent figure of merit *ZT* values for WS_2 samples with different amount of titanium doping in both directions (perpendicular and parallel to the pressing direction). The *ZT* values are dramatically enhanced by doping titanium. The optimum doping amount of titanium is 10% for the parallel direction and 5% for the perpendicular direction, respectively. For the pristine WS_2 sample, the $ZT_{//}$ and $ZT_{\perp}$ at 1000 K is 0.003 and 0.005, respectively. For doped Ti_xWS_2 composites, a maximum $ZT_{//}$ of 0.22 is achieved at 1000 K for $Ti_{0.1}WS_2$, which is 70 times larger than that in the pristine sample along the same direction. By comparing the maximum value of *ZT* along each direction, the anisotropic factor ($ZT_{//} / ZT_{\perp}$) is about 3, indicating the significant role of orientation on thermoelectric performance for layered TMDC materials. The anisotropy of *ZT* is primarily due to the anisotropy of thermal conductivity.

3.5 Textured structure of Ti_xWS_2

To unravel the mechanism of the modification of Ti-doping on thermoelectric properties and the anisotropic thermoelectric performance of Ti_xWS_2, we carried out XRD, SEM and TEM characterization to identify the microscopic structure. XRD pattern (Fig. 6(a)) along the parallel direction to the pressing direction indicates that pure WS_2 phase is formed for pristine sample after SPS process. Even after doping Ti, WS_2 phase is still maintained, which is also corroborated by TEM characterization (Fig. S1, Supporting Information).With increasing Ti concentration, TiW alloy phase builds up gradually(Fig. 6(b)). Small amount of WS_2 particles may decompose into W and S at high temperature during sintering and further react with Ti to form TiW alloy. TiW alloy, which is metallic with electrical conductivity about $1*10^6$ S/m,[18] can increase the electrical conductivity of Ti_xWS_2 composite. The molar ratio of TiW phase was calculated using relative intensity ratio method (see Supporting Information).[19] As shown in Table S1, the molar ratio of TiW phase is small and most Ti atoms are embedded into the lattice. It is worth noting that the distribution of titanium in Ti_xWS_2 samples is uniform, as suggested by the energy dispersive X-ray (EDX) elemental mapping (Fig. S2, Supporting Information).

Another distinct feature is that with increasing Ti amount, (00l) peaks become stronger and other peaks are suppressed, indicating the structure is textured along specific preferred directions. The degree of texturing can be quantified by using Lotgering orientation factor f of (00l) diffractions.[20] If f=1, perfect orientation occurs; if f=0, there is no preferred orientation. Interestingly, there exists a threshold concentration value for the orientation factor perpendicular to the pressing direction. Below 10%, the orientation factor is about 0.5, while above 10%, it jumps to about 0.8, which means that the preferred orientation occurs at this doping content. The sudden change of orientation factor f is corroborated by SEM images shown in Fig. 7. There is no preferential orientation for Ti_xWS_2 samples when x<0.1(Fig. 7(a, b and c)), while Ti_xWS_2 starts to align well along the pressing direction when the concentration of Ti is increased to 10% (Fig. 7(d, e and f)). At this stage, the perpendicular and parallel directions to the pressing direction coincide with the in-plane and cross-plane directions, respectively, which are commonly used for layered materials. XRD patterns (Fig. S4) along the direction perpendicular to the pressing direction further verify this phenomenon. As shown in Fig. S4 , the relative intensity of hkl (h≠0 or k≠0) peaks increases after Ti doping. The additive-induced alignment has been observed in other systems.[21] In this work, the second phase of TiW alloy formed during sintering may change the strain of materials and contribute to the ordering alignment. These structural evolutions observed here could explain well the change of electrical and thermal conductivity of WS_2 samples with Ti content.

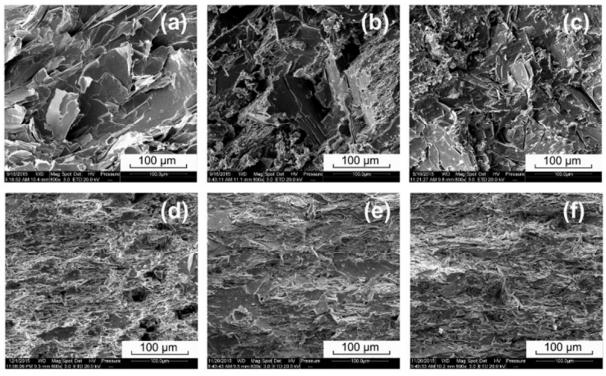

Fig. 7 Cross-sectional SEM images of Ti_xWS_2 after sintering with (a) x=0, (b)x=0.02, (c)x=0.05, (d)x=0.1, (e)x=0.15, (f)x=0.2 along the direction perpendicular to the pressing direction.

4 Conclusions

By introducing a facile doping scheme, the thermoelectric figure of merit *ZT* of WS_2 is dramatically improved to 0.22 at 1000 K, more than 70 times higher than that of pristine WS_2. Moreover, we reveal the anisotropy of thermoelectric performance of Ti doped WS_2 with superior thermoelectric efficiency appearing along the cross-plane direction due to the much lower thermal conductivity. Our studies may open an avenue for the exploration of thermoelectric

application of hot TMDC materials, such as MoS_2, WSe_2 and $MoSe_2$. Further improvement on the thermoelectric efficiency of TMDCs is expected by combining doping with other schemes like nanostructuring.

5 Acknowledgements

We thank Can Li for providing the access to Hall measurement instrument (HL5500PC). P. J. acknowledges financial support from the National Natural Science Foundation of China (NSFC) (Grant No. 21273228 and 51290272) and 100 Talents Program of the Chinese Academy of Sciences. W. Z. thanks NSFC Grant 21373201, NSFC Key Grant 21433014 and the "Strategic Priority Research Program" of the Chinese Academy of Sciences XDB10040304 and XDB 100202002 for the financial support.

References

1 (a) K. S. Novoselov, A. K. Geim, S. V. Morozov, D. Jiang, Y. Zhang, S. V. Dubonos, I. V. Grigorieva and A. A. Firsov, *Science*, 2004, **306**, 666-669; (b) A. Splendiani, L. Sun, Y. Zhang, T. Li, J. Kim, C.-Y. Chim, G. Galli and F. Wang, *Nano Lett*., 2010, **10**, 1271-1275; (c) K. F. Mak, C. Lee, J. Hone, J. Shan and T. F. Heinz, *Phys. Rev. Lett*., 2010, **105**, 136805; (d) B. Radisavljevic, A. Radenovic, J. Brivio, V. Giacometti and A. Kis, *Nat. Nanotechnol*, 2011, **6**, 147-150; (e) Q. H. Wang, K. Kalantar-Zadeh, A. Kis, J. N. Coleman and M. S. Strano, *Nat. Nanotechnol*., 2012, **7**, 699-712; (f) M. Chhowalla, H. S. Shin, G. Eda, L. J. Li, K. P. Loh and H. Zhang, *Nat. Chem*., 2013, **5**, 263-275; (g) J. T. Ye, Y. J. Zhang, R. Akashi, M. S. Bahramy, R. Arita and Y. Iwasa, *Science*, 2012, **338**, 1193-1196.

2 (a) D. Suh, D. Lee, C. Kang, I.-J. Shon, W. Kim and S. Baik, *J. Mater. Chem*., 2012, **22**, 21376-21381; (b) W. Huang, H. Da and G. Liang, *J. Appl. Phys.*, 2013, **113**, 104304; (c) W. Huang, X. Luo, C. K. Gan, S. Y. Quek and G. Liang, *Phys. Chem. Chem. Phys*., 2014, **16**, 10866-10874; (d) P. Jood, M. Ohta, H. Nishiate, A. Yamamoto, O. I. Lebedev, D. Berthebaud, K. Suekuni and M. Kunii, *Chem. Mater*., 2014, **26**, 2684-2692; (e) S. Kumar and U. Schwingenschloegl, *Chem. Mater*., 2015, **27**, 1278-1284.

3 (a) G. J. Snyder and E. S. Toberer, *Nat. Mater*., 2008, **7**, 105-114; (b) J. R. Sootsman, D. Y. Chung and M. G. Kanatzidis, *Angew. Chem. Int. Ed.*, 2009, **48**, 8616-8639.

4 (a) A. A. Balandin, S. Ghosh, W. Bao, I. Calizo, D. Teweldebrhan, F. Miao and C. N. Lau, *Nano Lett*., 2008, **8**, 902-907; (b) Y. Xu, Z. Li and W. H. Duan, *Small*, 2014, **10**, 2182-2199.

5 A. N. Gandi and U. Schwingenschloegl, *Chem. Mater*., 2014, **26**, 6628.

6 (a) G. K. Solanki, D. N. Gujarathi, M. P. Deshpande, D. Lakshminarayana and M. K. Agarwal, *Cryst. Res. Technol*., 2008, **43**, 179-185; (b) J.-Y. Kim, S. M. Choi, W.-S. Seo and W.-S. Cho, *B. Kor. Chem. Soc*., 2010, **31**, 3225-3227; (c) J. Y. Oh, J. H. Lee, S. W. Han, S. S. Chae, E. J. Bae, Y. H. Kang, W. J. Choi, S. Y. Cho, J.-O. Lee, H. K. Baik and T. I. Lee, *Energy Environ. Sci.*, 2016, DOI: 10.1039/C5EE03813H.

7 H.-S. Kim, Z. M. Gibbs, Y. Tang, H. Wang and G. J. Snyder, *APL Mater*., 2015, **3**, 041506.

8 G. Kresse and J. Furthmüller, *Phys. Rev. B*, 1996, **54**, 11169-11186.

9 J. P. Perdew, K. Burke and M. Ernzerhof, *Phys. Rev. Lett*., 1996, **77**, 3865-3868.

10 S. Grimme, *J. Comput. Chem*., 2006, **27**, 1787-1799.

11 J. Heyd and G. E. Scuseria, *J. Chem. Phys.*, 2004, **121**, 1187-1192.

12 (a) J. M. Ziman, *Principles of the theory of solids*, Cambridge University Press, Cambridge, England, 1972, p. 211; (b) P. B. Allen, W. E. Pickett and H. Krakauer, *Phys. Rev. B*, 1988, **37**, 7482-7490.

13 G. K. H. Madsen and D. J. Singh, *Comput. Phys. Commun.*, 2006, **175**, 67-71.

14 K. Peng, X. Lu, H. Zhan, S. Hui, X. Tang, G. Wang, J. Dai, C. Uher, G. Wang and X. Zhou, *Energy Environ. Sci.*, 2016, **9**, 454-460.

15 (a) F. D. Rosi, *Solid State Electron.*, 1968, **11**, 833-868; (b) J. Suh, K. M. Yu, D. Fu, X. Liu, F. Yang, J. Fan, D. J. Smith, Y.-H. Zhang, J. K. Furdyna, C. Dames, W. Walukiewicz and J. Wu, *Adv. Mater.*, 2015, **27**, 3681-3686.

16 (a) L. D. Zhao, B. P. Zhang, J. F. Li, H. L. Zhang and W. S. Liu, *Solid State Sci.*, 2008, **10**, 651-658; (b) X. Yan, B. Poudel, Y. Ma, W. S. Liu, G. Joshi, H. Wang, Y. Lan, D. Wang, G. Chen and Z. F. Ren, *Nano Lett*., 2010, **10**, 3373-3378; (c) J. Sui, J. Li, J. He, Y.-L. Pei, D. Berardan, H. Wu, N. Dragoe, W. Cai and L.-D. Zhao, *Energy Environ. Sci.*, 2013, **6**, 2916-2920.

17 (a) P. G. Klemens, *Solid State Physics*, eds. F. Seitz and D. Turnbull, Academic Press, 1958, vol. 7, p. 1-98; (b) G. A. Slack, *Solid State Physics*, eds. H. Ehrenreich, F. Seitz and D. Turnbull, Academic Press, New York, 1979, vol. 34, p. 1-71; (c) E. S. Toberer, A. Zevalkink and G. J. Snyder, *J. Mater. Chem.*, 2011, **21**, 15843-15852; (d) E. S. Toberer, L. L. Baranowski and C. Dames, *Annu. Rev. Mater. Res.*, 2012, **42**, 179-209.

18 Y. Sakurai, Y. Takeda, S. Ikeda, and Y. Sakamoto, *Phys. Status Solidi C*, 2014, **11**, No. 9, 1423–1426.

19 F. H. Chung, *J. Appl. Cryst.*, 1974, **7**, 519-525

20 F. K. Lotgering, *J. Inorg. Nucl. Chem.*, 1959, **9**, 113-123.

21 (a) Q. W. Huang, L. H. Zhu, J. Xu, P. L. Wang, H. Gu and Y. B. Cheng, *J. Eur. Ceram. Soc.*, 2005, **25**, 957-962; (b) P. Jood, M. Ohta, O. I. Lebedev and D. Berthebaud, *Chem. Mater.*, 2015, **27**, 7719-7728.

Title:
Enhancement of Anisotropic Thermoelectric Performance of Tungsten Disulfide by Titanium Doping

Zhiwei Huang,[a,d,§] Tianmin Wu,[c,§] Shuang Kong,[a,d] Qinglong Meng,[a] Wei Zhuang,[*,b,e] Peng Jiang,[*,a] Xinhe Bao[*,a]

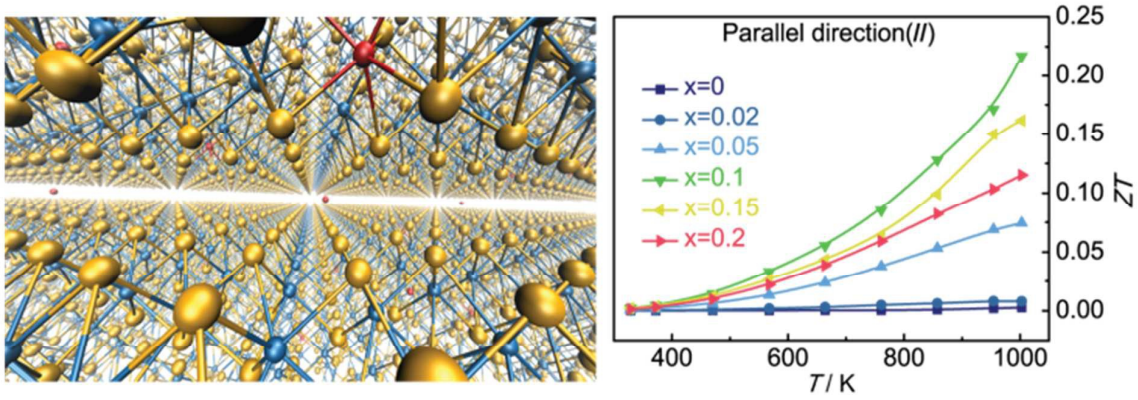

The table of contents: Using facile doping strategy, the thermoelectric performance of tungsten disulfide is enhanced up to 40 times. Our study will stimulate further exploration of the potential applications in thermoelectrics for transition metal dichalcogenide semiconductors and other two-dimensional materials.